Journal of Power Sources 196 (2011) 700–708

Contents lists available at ScienceDirect

Journal of Power Sources

journal homepage: www.elsevier.com/locate/jpowsour

Seal glass compatibility with bare and $(Mn,Co)_3O_4$ coated Crofer 22 APU alloy in different atmospheres

M.K. Mahapatra, K. Lu*

Department of Materials Science and Engineering, Virginia Polytechnic Institute and State University, Blacksburg, VA 24061, USA

ARTICLE INFO

Article history:
Received 2 June 2010
Received in revised form 21 July 2010
Accepted 24 July 2010
Available online 3 August 2010

Keywords:
Seal glass
Interconnect
$(Mn,Co)_3O_4$ coating
Diffusion
Chemical reaction
Devitrification

ABSTRACT

To prevent gas mixing and leakage during solid oxide fuel/electrolyzer cell operation, the interconnect/seal glass interface should bond well and remain stable. A $SrO–La_2O_3–Al_2O_3–SiO_2$ (SABS-0) seal glass has been bonded to bare Crofer 22 APU alloy and $(Mn,Co)_3O_4$ coated Crofer 22 APU alloy. The stability of the interconnect/SABS-0 interface has been studied in air and H_2/H_2O atmospheres at 800 °C for 1000 h. The interconnect/seal glass interaction involves the oxidation of the bare and $(Mn,Co)_3O_4$ coated Crofer 22 APU alloy surfaces, inter-diffusion of elements, chemical reaction, and the devitrification of the SABS-0 glass. The study shows that the thermal treatment atmosphere greatly affects the interfacial stability of both bare Crofer 22 APU/SABS-0 and $(Mn,Co)_3O_4$ coated Crofer 22 APU/SABS-0 samples. The interfacial stability is better in the H_2/H_2O atmosphere for both samples. The instability of the $(Mn,Co)_3O_4$ coating under the thermal treatment conditions degrades the interfacial compatibility of the $(Mn,Co)_3O_4$ coated Crofer 22 APU/SABS-0 sample.

1. Introduction

Seal glasses are essential for joining solid oxide fuel/electrolyzer cell (SOFC/SOEC) components (electrodes, electrolyte, and interconnect) in order to prevent leakage and mixing of gases in a fuel/electrolyzer cell stack. Among all the SOFC/SOEC components, the interconnect/seal glass interface is the most crucial and exposed to simultaneous oxidizing and wet (can be >50% H_2O) reducing environments. To be hermetic, the interconnect/seal glass interface should be pore- and crack-free and stable for the entire cell operation period at 650–900 °C [1]. Several requirements need to be met in order to obtain a hermetic interconnect/seal glass interface [1]. First, the seal glass should adhere to and bond strongly with the metallic interconnect. Second, the interface should be thin in order to minimize the residual stress at the interface. Third, the interaction (inter-diffusion and chemical reaction) between the interconnect and the seal glass should be minimal. Fourth, diffusion of chromium and iron into the seal glass and the seal glass elements into the interconnect should be avoided.

The interfacial stability depends on the compositions of the seal glass and the interconnect as well as the cell operating conditions [1]. Alkaline earth oxide-containing borosilicate and silicate glasses are the most investigated seal glasses. BaO–CaO–borosilicate, SrO–CaO–borosilicate, and BaO–CaO–silicate glass systems react with the interconnect and induce cracks at the interface due to the formation of detrimental chromates of high CTE ($21.0–23.0 \times 10^{-6}\ K^{-1}$) [2–6]. Crofer 22 APU alloy is the most preferred metallic interconnect [7]. $(Mn,Co)_3O_4$ coated Crofer 22 APU alloy (abbreviated as MC Crofer 22 APU alloy) is also studied in order to reduce 'chromium poisoning' [8]. Cell operating conditions such as atmosphere, temperature, and time affect the interfacial stability [1,9–11]. Air promotes chromate phase formation and H_2/H_2O atmosphere promotes iron- and chromium-containing phase formation at the interface [6,12]. The interfacial layer can undesirably increase with thermal treatment time. For example, the interfacial thickness increases from 10 μm for the as-bonded Crofer 22 APU/BaO–CaO–borosilicate glass to 76 μm after thermal treatment in air at 750 °C for 200 h [13]. However, most of the interconnect/seal glass interfacial studies have been conducted in air or low water content (3%) reducing atmosphere for the bare Crofer 22 APU alloy. Limited reports are available for the coated Crofer 22 APU alloy/seal glass interface or the interfacial stability in high water content reducing atmosphere [14].

In our previous studies, it has been shown that a $SrO–La_2O_3–Al_2O_3–SiO_2$ glass (SABS-0) is compatible with the Crofer 22 APU alloy at 800 °C regardless of thermal treatment atmospheres but its compatibility is inferior with the MC Crofer 22 APU alloy [11,14]. An interfacial thickness of ≤3 μm is maintained. The diffusion distances of the alloy elements (≤10 μm) and the SABS-0 glass elements (≤3 μm) are also almost constant regardless of the thermal treatment conditions. The superior interfacial compatibility is attributed to the desirable properties of the SABS-0 seal glass [15,16]. However, these interfacial compatibility studies were carried out only for 100 h.

* Corresponding author. Tel.: +1 540 231 3225; fax: +1 540 231 8919.
E-mail address: klu@vt.edu (K. Lu).

0378-7753/$ – see front matter © 2010 Elsevier B.V. All rights reserved.
doi:10.1016/j.jpowsour.2010.07.084

For long-term interfacial compatibility study, this work is focused on both bare and MC Crofer 22 APU alloy interfaces with the SABS-0 seal glass in air and high water content H_2 atmospheres at 800 °C for 1000 h. The effect of the $(Mn,Co)_3O_4$ coating on the interfacial compatibility is also studied along with the thermal treatment atmospheres.

2. Experimental procedure

2.1. Glass preparation

The SABS-0 glass was prepared with conventional glass manufacturing process. $SrCO_3$ (99.9%, Sigma–Aldrich, St. Louis, MO), La_2O_3 (99.98%), Al_2O_3 (99.95%), and SiO_2 (99.8%) (all oxides were from Alfa Aesar, Ward Hill, MA) at designed ratios were mixed in a ball mill for overnight. The mixed powders were heated in a platinum crucible in a box furnace (Lindberg, Model No. 51314, Watertown, WI) to 1100 °C and kept there for 1 h for $SrCO_3$ to decompose. After that, the mixture was heated to 1400 °C for 4 h. The heating rate was 10 K min^{-1}. The molten glass was quenched into a graphite mold.

2.2. Sample preparation for interfacial study

Bare Crofer 22 APU samples (ThyssenKrupp VDM, Germany) were polished to optical finish to remove oxidized surface layer, if any, and to obtain a scratch-free flat surface. The polished samples were cleaned in an ultrasonic bath with water followed by acetone before being dried and wiped with acetone. In addition, some Crofer 22 APU alloy samples were coated with ~2 μm thick $(Mn,Co)_3O_4$ spinel by a DC electrodeposition method [17]. The composition of the Crofer 22 APU alloy was provided before [9,11].

Clean and flat SABS-0 glass pieces were put on the polished bare Crofer 22 APU alloy and the MC Crofer 22 APU alloy surfaces. The samples were thermally treated at 960 °C for 30 min in argon in order to bond the SABS-0 glass with the interconnect samples without detrimental $SrCrO_4$ phase formation. The bonded samples were thermally treated at 800 °C in air and H_2/H_2O atmosphere for 1000 h. The H_2/H_2O atmosphere was created by passing hydrogen gas through a water bath. The temperature of the water bath was maintained at 83 ± 2 °C to obtain approximately 50% water vapor [18]. The same heating and cooling rates of 3 K min^{-1} were used for all the thermal treatment conditions.

2.3. Characterization

The cross sections of the as-bonded and the thermally treated Crofer 22 APU/SABS-0 and MC Crofer 22 APU/SABS-0 samples were finely polished to optical finish. A scanning electron microscope (SEM, Quanta 600 FEG, FEI Company, Hillsboro) was used to examine the interfacial morphologies of the Crofer 22 APU/SABS-0 and MC Crofer 22 APU/SABS-0 samples. The EDS module (Bruker AXS, MiKroanalysis, Gmbh, Berlin, Germany) attached to the SEM was used for composition analysis. The elemental distribution along the interface was determined by standardless EDS spot analysis, line scan, and area mapping. The EDS scans were collected for 60 s for spot analysis of different phases, 240 s for line scan analysis across the interface, and 600 s for area mapping with 15 kV accelerating voltage. Three scans were taken for the spot and line scan analyses and the averaged results were reported.

3. Results

3.1. Microstructures at the interface

3.1.1. Crofer 22 APU/SABS-0 interface

Fig. 1(a) presents the microstructure of the as-bonded Crofer 22 APU/SABS-0 sample while Fig. 1(b) and (c) presents the microstructures of the thermally treated Crofer 22 APU/SABS-0 samples in the air and H_2/H_2O atmospheres, respectively. In the images, the left side is the Crofer 22 APU alloy and the right side is the SABS-0 glass. For all the samples, a well-bonded interface is obtained. The thin gap at the interface is likely an artifact caused by the lateral

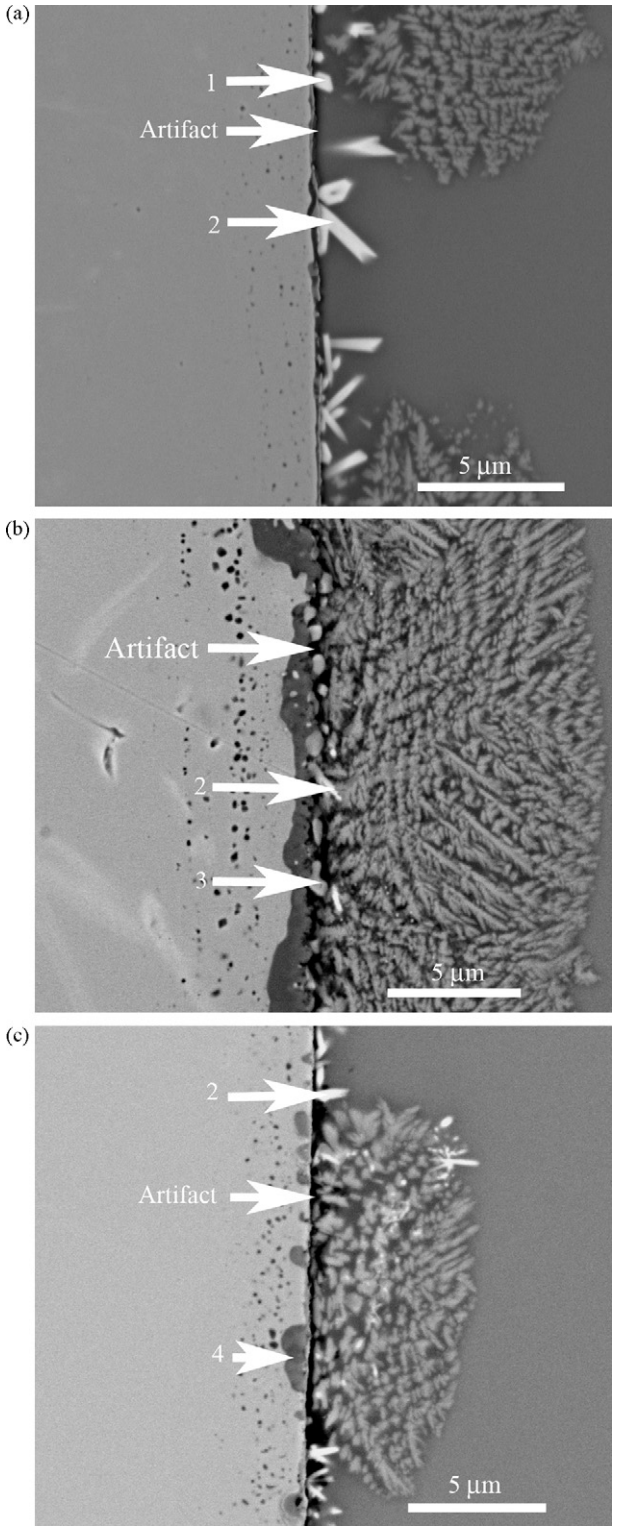

Fig. 1. Cross section SEM images of Crofer 22 APU/SABS-0 samples: (a) as-bonded, (b) thermally treated for 1000 h at 800 °C in air, and (c) thermally treated for 1000 h at 800 °C in H_2/H_2O atmosphere. The left side is the Crofer 22 APU alloy and the right side is the SABS-0 glass. The numbers corresponds to the numbers used in Sections 3 and 4.

spreading of the electron beam during the imaging process [19]. The microstructures can be divided into three regions near the interface: the Crofer 22 APU alloy side, the interface, and the partially devitrified SABS-0 glass side.

Tiny dark spots ($\ll$1 μm) distribute on the Crofer 22 APU alloy side at <5 μm from the interface with a similar orientation for all the samples. The size and spread are the largest for the air treated sample.

The interfacial morphology and thickness differ for the as-bonded, air treated, and H_2/H_2O treated samples. On the Crofer 22 APU alloy side near the interface, the as-bonded sample has a clean and even Crofer 22 APU alloy surface. For the air treated sample, a continuous dark gray layer is present. For the H_2/H_2O treated sample, dark gray granular phases are visible (marked as 4 in Fig. 1(c)). The interface is very thin for the as-bonded sample ($\ll$1 μm) and shows almost no change except for the increased amount of the tiny dark spots and the dark granular phases for the H_2/H_2O atmosphere treated couple. For the air treated sample, however, the interface is the thickest (although <2 μm) and equiaxed, light gray colored phases ($\leq$1 μm) are scattered at the interface (marked as 3 in Fig. 1(b)).

On the SABS-0 glass side, equiaxed (marked as 1) and elongated (marked as 2) bright phases are present near the interface for the as-bonded sample (Fig. 1(a)) but only elongated phases to a very limited extent are observed for the thermally treated samples. Dendritic phases are observed for all the samples and the amount is again the highest for the air treated sample. Nonetheless, none of the devitrified phases extend beyond 10 μm from the interface.

3.1.2. MC Crofer 22 APU/SABS-0 interface

Fig. 2(a) presents the microstructure of the as-bonded MC Crofer 22 APU/SABS-0 sample while Fig. 2(b) and (c) presents the microstructures of the thermally treated MC Crofer 22 APU/SABS-0 samples in the air and H_2/H_2O atmospheres, respectively. In the images, the left side is the Crofer 22 APU alloy and the right side is the SABS-0 glass. The microstructures can be discussed again from three aspects: the Crofer 22 APU alloy side near the interface, the interface including the MC layer, and the SABS-0 glass side near the interface.

On the Crofer 22 APU alloy side, dark spots with larger sizes than those for the bare Crofer 22 APU/SABS-0 samples are observed at <8 μm from the interface for all the samples. The dark spots grow larger and spread more for the thermally treated samples, with the highest extent for the air treated sample.

Two distinct interfaces are observed: one between the Crofer 22 APU alloy and the MC layer (marked as 1) for all the samples and the other between the MC layer and the SABS-0 glass (marked as 3) for the as-bonded and air treated samples. The MC layer is marked as 2 in Fig. 2. The interface on the Crofer 22 APU side (marked as 1) contains pores for all the samples. The interface is smoother for the as-bonded sample than for the thermally treated samples. Granular phases (marked as 4) are observed for the air and H_2/H_2O atmosphere treated samples. For the H_2/H_2O atmosphere treated sample, the interface (marked as 1) and the granular phases (marked as 4) are connected. The MC layer (marked as 2) is porous and its thickness decreases from the as-bonded sample to the air treated sample. For the H_2/H_2O atmosphere treated sample, the MC layer is invisible but a layer containing bright phases (marked as 5) is observed. The interface on the SABS-0 glass side (marked as 3) is observed only for the as-bonded and air treated samples.

Dendritic phases are observed on the SABS-0 glass side for all the samples. The thermal treatment atmospheres do not affect the devitrification extent. The devitrified phases spread less than 15 μm from the interface. The dark spots in the devitrified SABS-0 glass are likely pores. Overall, the MC Crofer 22 APU/SABS-0 sam-

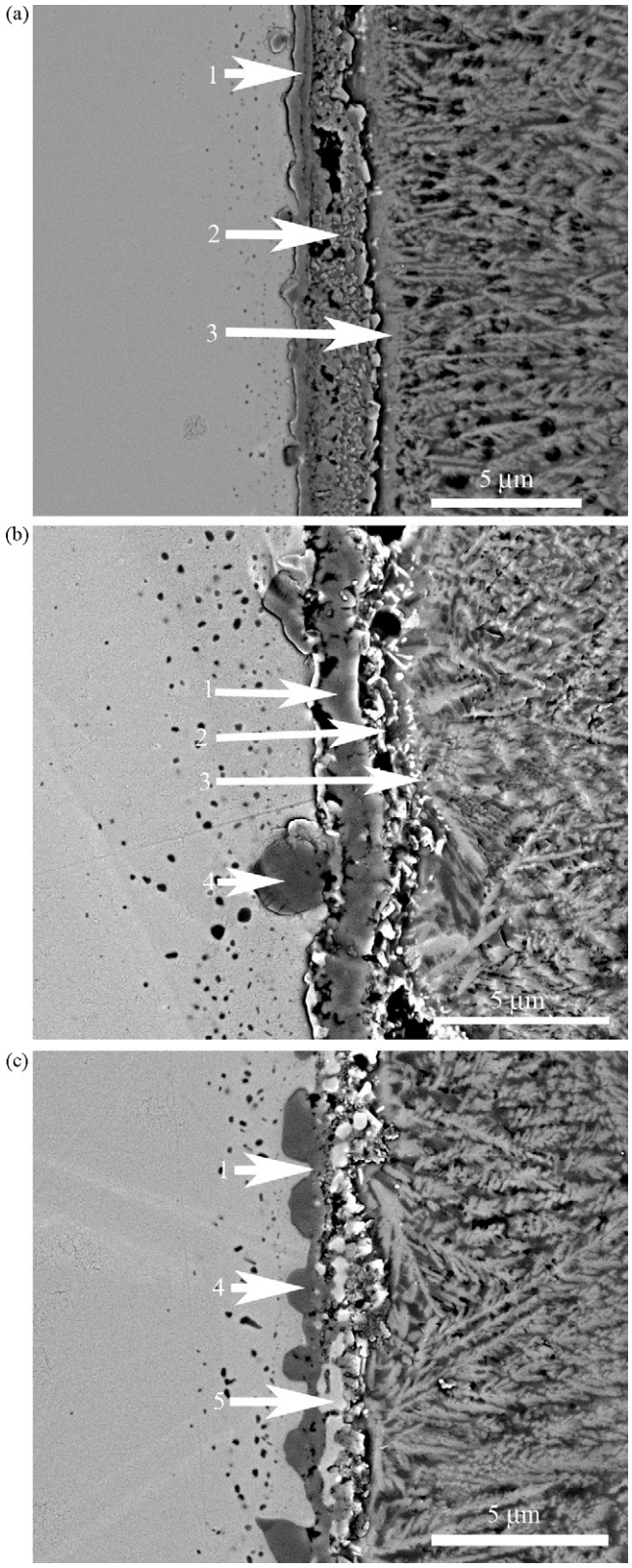

Fig. 2. Cross section SEM images of MC Crofer 22 APU/SABS-0 samples: (a) as-bonded, (b) thermally treated for 1000 h at 800 °C in air, and (c) thermally treated for 1000 h at 800 °C in H_2/H_2O atmosphere. The left side is the MC Crofer 22 APU alloy and the right side is the SABS-0 glass. The numbers corresponds to the numbers used in Sections 3 and 4.

Table 1
EDS spot analysis results of Crofer 22 APU/SABS-0 interfaces.

		Fe	Cr	Mn	Ti	O	Si	Sr	La	Al
Crofer 22 APU		75.6	24.0	0.4	0	0	0	0	0	0
As-bonded	Dark spot	65.0	20.8	0.5	3.0	10.8	0	0	0	0
	Interface	37.4	16.2	1.3	0.3	34.0	5.3	4.3	0.9	0
	1	7.7	10.0	2.0	0.2	51.0	13.6	8.0	4.5	3.0
	2	1.3	2.0	0.6	0.4	62.6	15.7	9.0	5.2	3.0
Air 1000 h	Dark spot	51.6	17.4	0.4	10.6	18.4	0	0	0	1.6
	Interface	7.5	26.8	0.9	0	59.6	1.2	0	0	0.5
	2	9.0	3.3	0.5	0	47.8	19.4	9.6	6.9	3.4
	3	58.7	12.5	1.5	0	19.7	3.6	1.7	0.7	1.6
H_2/H_2O 1000 h	Dark spot	63.7	20.6	0.4	6.1	9.5	0	0	0	0.3
	2	3.3	3.7	0.7	0	51.6	18.7	11.1	7.0	3.8
	4	22.5	23.0	3.1	2.1	46.3	0.7	1.7	0	0.6

ples (Fig. 2) have more extensive glass devitrification than the bare Crofer 22 APU/SABS-0 samples (Fig. 1).

3.2. Elemental distribution at the interface

The EDS analysis cannot provide highly accurate quantitative results because of the spatial resolution limitation of the secondary X-rays (≥1 μm) and the fluorescence effect [19]. The spatial resolution is generally believed to be 1 μm [19]. Nonetheless, qualitative information can be obtained to understand the relative trend in the compositional difference among the different phases. In this study, the compositions of the different phases are analyzed and reported in at%.

3.2.1. EDS spot analysis

3.2.1.1. Crofer 22 APU/SABS-0 interface. The EDS spot analysis results for the Crofer 22 APU/SABS-0 interfaces are shown in Table 1. For the as-bonded sample, the tiny dark spots on the Crofer 22 APU alloy side consist of Fe 65.0, Cr 20.8, Mn 0.5, Ti 3.0, and O 10.8. For the thermally treated samples, the tiny dark spots have approximately the same composition but contain ≤1.5% Al and ≥6.5% Ti. The higher titanium content indicates that the dark spots are titanium-enriched oxide after the thermal treatment. The interface of the as-bonded sample consists of Fe 37.4, Cr 16.2, Mn 1.3, Ti 0.3, Si 5.3, Sr 4.3, La 0.9, and O 34. The interface of the air treated sample is enriched in chromium (Cr 26.8). The bright granular phases at the interface (marked as 3 in Fig. 1(b)) consist of Fe 58.7, Cr 12.5, Mn 1.5, Si 3.6, Sr 1.7, La 0.7, Al 1.6, and O 19.7. For the H_2/H_2O atmosphere treated sample, the interface is so thin that its composition cannot be reliably detected from the EDS analysis; the granular phases on the Crofer 22 APU alloy side near the interface contain Fe 22.5, Cr 23.0, Mn 3.1, Ti 2.1, Si 0.7, Sr 1.7, Al 0.6, and O 46.3.

On the SABS-0 glass side, the equiaxed bright phases (marked as 1 in Fig. 1(a)) have higher Crofer 22 APU alloy contents, except for Ti, than the elongated phases (marked as 2 in Fig. 1(a)) for the as-bonded sample. The bright phases have similar compositions for the thermally treated samples but with higher contents of the SABS-0 glass elements. For the air treated sample, the dendritic phases cannot be distinguished from the glass phase in-between them. For the as-bonded and H_2/H_2O atmosphere treated samples, the dendritic phases have higher strontium and lanthanum contents but lower aluminum content than the glass phase. For all the samples, the dendritic phases and the glass matrix near the interface also contain small amounts of iron and chromium.

3.2.1.2. MC Crofer 22 APU/SABS-0 interface. The EDS spot analysis results for the MC Crofer 22 APU/SABS-0 interfaces are shown in Table 2. For the as-bonded sample, the dark spots on the Crofer 22 APU side consist of Fe 69.7, Cr 22.4, Mn 0.9, Ti 2.7, and O 4.3; the interface on the Crofer 22 APU side (marked as 1 in Fig. 2) consists of Fe 31.1, Cr 25.2, Mn 1.8, Ti 0.6, Co 2.1, and O 39.2. For the thermally treated samples, the dark spots have similar compositions to the as-bonded sample but with ≤0.5% Al, ≤0.5% Si, and 6–10% Ti; Co is absent but ≤1% Si, Sr, and Al are present at the interface along with 2–8% Fe, 26–28% Cr, and 10–13% Mn. The Mn:Cr ratio increases from ~1:12 for the as-bonded sample to ~1:1.5 for the thermally treated samples. For the air and H_2/H_2O atmosphere treated sample, the granular phases (marked as 4) have similar compositions to those of the interface 1 for the air treated sample and the H_2/H_2O atmosphere treated sample. For the as-bonded sample, the MC layer (marked as 2 in Fig. 2(a)) mainly consists of Fe 5.6, Cr 16.9, Mn 6.8, Co 25.7, Sr 2.0, Al 0.8, and O 42.2 with ~1:4 Mn:Co ratio. For the air treated sample, the MC layer (marked as 2 in Fig. 2(b)) consists of Fe 9.7, Cr 4.6, Mn 5.7, Co 50.4, Si 4.3, Sr 4.2, La 0.3, Al 2.3, O 18.6, noting the Mn:Co ratio is ~1:8. For the H_2/H_2O atmosphere treated sam-

Table 2
EDS spot analysis results of MC Crofer 22 APU/SABS-0 interfaces.

		Fe	Cr	Mn	Ti	Co	O	Si	Sr	La	Al
As-bonded	Dark spot	69.7	22.4	0.9	2.7	0	4.3	0	0	0	0
	1	31.1	25.2	1.8	0.6	2.1	39.2	0	0	0	0
	2	5.6	16.9	6.8	0	25.7	42.2	0	2.0	0	0.8
	3	0.9	2.3	4.2	0	9.6	53.4	14.9	10.5	2.3	1.8
Air 1000 h	Dark spot	60.5	20.3	0.9	5.7	0	11.7	0.2	0	0	0.6
	1	2.0	23.1	10.0	0	1.6	61.6	0.6	0.6	0	0.5
	2	9.7	4.6	5.7	0	50.4	18.6	4.3	4.2	2.3	1.8
	3	0.8	1.3	7.5	0	2.3	55.5	17.2	10.3	3.0	2.3
	4	2.4	33.9	15.4	0	0	47.4	0	0	0	0.4
H_2/H_2O 1000 h	Dark spot	53.4	17.5	1.0	10.5	0	16.7	0.4	0	0	0.5
	1	8.3	25.5	10.1	0.6	0	53.9	0.3	1.1	0	0.2
	4	3.2	27.5	11.7	1.0	0	55.6	0.3	0	0	0.2
	5	3.9	21.6	9.4	0	2.6	53.5	3.3	3.8	0.6	1.2

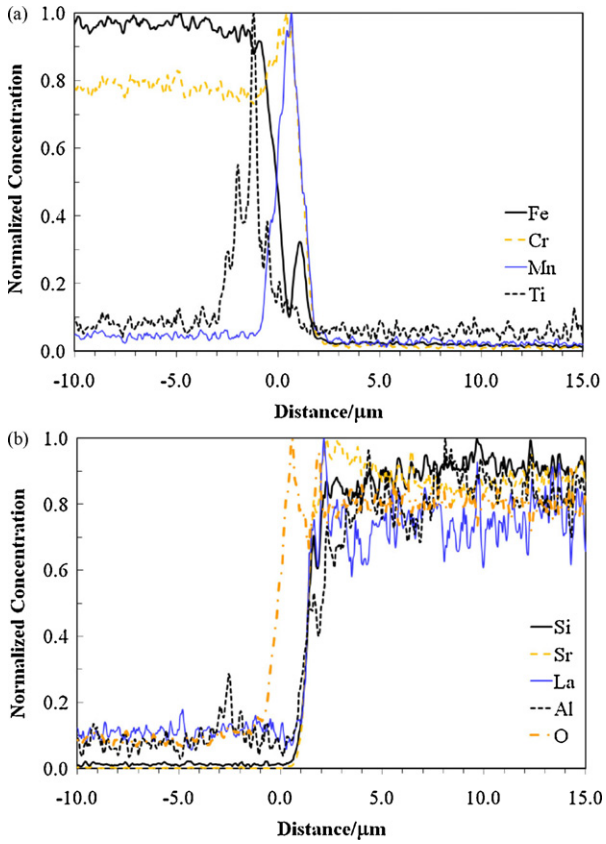

Fig. 3. Elemental concentration profiles of the 1000 h air treated Crofer 22 APU/SABS-0 sample: (a) Crofer 22 APU alloy elements, and (b) SABS-0 glass elements. The negative side on the *X*-axis indicates the Crofer 22 APU alloy side and the positive side indicates the SABS-0 glass side.

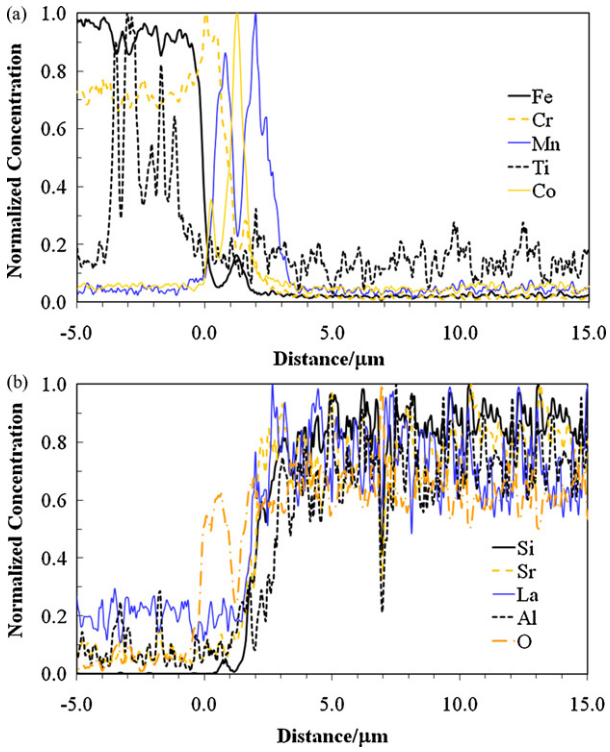

Fig. 4. Elemental concentration profiles of the 1000 h air treated MC Crofer 22 APU/SABS-0 sample: (a) MC Crofer 22 APU alloy elements, and (b) SABS-0 glass elements. The negative side on the *X*-axis indicates the MC Crofer 22 APU alloy side and the positive side indicates the SABS-0 glass side.

ple, the MC layer is absent but the bright phases (marked as 5) have different compositions. For the as-bonded sample, the interface on the SABS-0 side (marked as 3) consists of Fe 0.9, Cr 2.3, Mn 4.2, Co 9.6, Si 14.9, Sr 10.5, La 2.3, Al 1.8, and O 53.4 with the Mn:Co ratio at ~1:2. For the air treated sample, the interfacial composition on the SABS-0 glass side (marked as 3) is similar to that of the as-bonded sample but the Mn:Co ratio changes to ~3:1.

For all the samples, the dendritic phases on the SABS-0 glass side have higher strontium and lanthanum contents but lower aluminum content than the glass phase. The dendritic phases and the glass matrix in-between near the interface also contain small amounts of iron, chromium, and cobalt.

3.2.2. EDS line scan analysis

The elemental concentration profiles of the Crofer 22 APU/SABS-0 and MC Crofer 22 APU/SABS-0 samples are shown in Figs. 3 and 4, respectively, only for the air treated condition (the most severe interaction case) for brevity. '0' on the *x* axis indicates the boundary between the alloy and the interface. The left (negative) side is the alloy and the right (positive) side is the SABS-0 glass. The *y* axis shows the normalized concentrations of the elements. The concentration profiles, except for manganese, titanium, and cobalt, are 'S' shaped with two diffusion tails: one at the high concentration end and the other at the low concentration end. This means the inter-diffusion of the Crofer 22 APU alloy and the SABS-0 glass elements occurs across the interface [20]. The concentration profiles of manganese, titanium, and cobalt show sharp humps rather than 'S' shape. Oscillations in the concentration profiles are observed for all the SABS-0 glass elements with several possible reasons: interaction between the X-rays of different elements, low concentrations of the SABS-0 glass elements, low density of the SABS-0 glass, and the compositional difference between the devitrified and glass phases [19]. However, approximate diffusion distances of the elements can be determined from the inflection points of the 'S' shaped diffusion profiles [20].

3.2.2.1. Crofer 22 APU/SABS-0 interface. As shown in Fig. 3, iron in the Crofer 22 APU alloy diffuses 1–3 μm into the SABS-0 glass for all the samples but the diffusion distance increases from the as-bonded, the H_2/H_2O atmosphere treated, to the air treated conditions. For the air treated sample, a hump in the iron concentration profile is observed on the SABS-0 glass side, consistent with the iron enriched bright phases (marked as 3 in Fig. 1(b)). Chromium diffuses ~5, ~6, and ~8 μm, respectively, into the SABS-0 glass for the as-bonded, air treated, and H_2/H_2O atmosphere treated samples. For the thermally treated samples, a hump in the chromium concentration profile is observed on the Crofer 22 APU alloy side near the interface. Manganese concentration is highest at/near the interface. Titanium concentration is highest beneath the highest manganese concentration location, consistent with the high manganese content at the interface and the high titanium content in the dark spots on the Crofer 22 APU alloy side. The SABS-0 glass elements (Si, Sr, La, Al, and O) diffuse 2–4 μm into the Crofer 22 APU alloy side for the as-bonded, air treated, and H_2/H_2O treated samples, respectively.

3.2.2.2. MC Crofer 22 APU/SABS-0 interface. As shown in Fig. 4, iron in the Crofer 22 APU alloy diffuses 3–4 μm into the SABS-0 glass for the as-bonded sample but decreases to 2–3 μm for the thermally treated conditions. A hump is observed in the iron concentration profiles on the SABS-0 glass side for the thermally treated samples. Chromium diffuses ~3 μm for the as-bonded sample and ~2 μm for the thermally treated samples. The iron diffusion distance is larger and the chromium diffusion distance is smaller than those

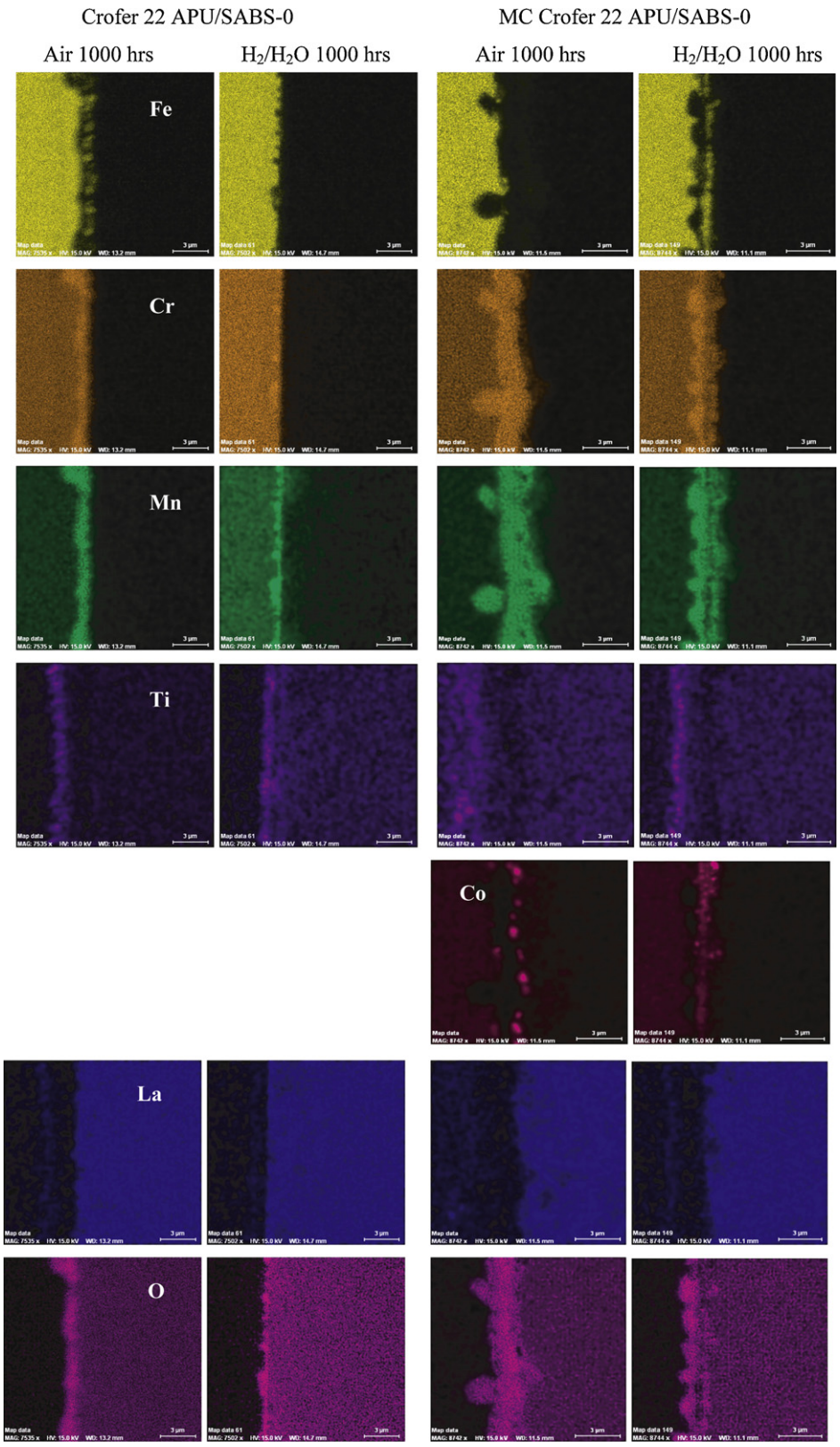

Fig. 5. Elemental maps for the Crofer 22 APU/SABS-0 and MC Crofer 22 APU/SABS-0 couples thermally treated at 800 °C for 1000 h in air and H_2/H_2O atmospheres.

for the bare Crofer 22 APU alloy, with the understanding that the MC coating might make this comparison less certain. Humps are observed for manganese, titanium, and cobalt concentration profiles due to their highest concentrations at/near the interface. The hump for the manganese concentration profile extends to ~4 μm, a total thickness of the MC layer and the interfaces on the Crofer 22 APU alloy and the SABS-0 glass sides. The titanium hump is beneath the manganese hump, consistent with the titanium enriched dark spots beneath the interface. The cobalt hump width approximately matches with the MC layer thickness for the as-bonded sample but

decreases for the thermally treated samples. For the H_2/H_2O treated sample, the cobalt hump moves to the SABS-0 glass side. Silicon, strontium, and oxygen in the SABS-0 glass diffuse 2–3 μm into the MC Crofer 22 APU alloy. The diffusion distances for lanthanum and aluminum are 1.5 and 3.5 μm, respectively, with extensive oscillations in their concentration profiles.

3.2.3. Elemental maps

For a better understanding of the elemental distribution across the interface, EDS maps are shown in Fig. 5 for selected elements of the thermally treated samples. For both Crofer 22 APU/SABS-0 and MC Crofer 22 APU/SABS-0 samples, silicon, strontium, and aluminium maps are not given because of the absence of any distinguishable features.

For the air treated Crofer 22 APU/SABS-0 sample, localized Fe-rich region on the SABS-0 glass side superimposes with the gray equiaxed phases in the microstructure (marked as 3 in Fig. 1(b)). For the H_2/H_2O treated sample, chromium and manganese are enriched at the interfaces for all the samples and the enriched regions overlap with the granular phases on the Crofer 22 APU alloy side (marked as 4 in Fig. 1(c)); iron is depleted in the granular phases. For all the Crofer 22 APU/SABS-0 couples, the titanium-enriched region is observed beneath the manganese-enriched region; lanthanum is locally enriched on the SABS-0 glass side near the interface and the enriched regions superimpose with the bright spots in the microstructure (Fig. 1), consistent with the EDS spot analysis; oxygen accumulates at the interface. These observations are consistent with the EDS spot and line scan analyses.

For the air and H_2/H_2O atmosphere treated MC Crofer 22 APU/SABS-0 samples, iron is depleted at the interface and in the granular phases on the Crofer 22 APU alloy side but enriched in the bright phases (marked as 5 in Fig. 2(c)) at the interface. Chromium and manganese are enriched in the granular phases on the Crofer 22 APU alloy side and at the interfaces for all the samples. Titanium is enriched beneath the manganese enriched interfaces. The cobalt enriched regions are observed at the interface near the SABS-0 glass for the thermally treated samples. For all the MC Crofer 22 APU/SABS-0 samples, lanthanum distributes homogeneously in the SABS-0 glass and oxygen accumulates at the interface. All these observations are consistent with the EDS spot and line scan analyses.

4. Discussion

4.1. Crofer 22 APU/SABS-0 samples

The interfacial behaviors of the Crofer 22 APU/SABS-0 samples in different atmospheres can be discussed from the combined effect of the Crofer 22 APU alloy oxidation, the chemical reaction between the alloy and the SABS-0 glass, the diffusion of the alloy and glass elements, and the SABS-0 glass devitrification.

For the Crofer 22 APU alloy, manganese addition is intended to improve oxidation resistance and suppress chromium vaporization and titanium addition is intended to improve electrical conductivity. However, the lower concentration, lower diffusivity, and higher oxygen affinity of titanium than manganese favor the internal oxidation of titanium [21]. Subsequently, the titanium-enriched tiny dark spots form on the Crofer 22 APU alloy side by internal oxidation of titanium (Fig. 1), supported by the hump near the interface in the titanium concentration profile and titanium enrichment near the interface in the elemental maps. Aluminum is an impurity in the Crofer 22 APU alloy. After the 1000 h thermal treatment, aluminium also oxidizes internally because of its higher stability than TiO_2 and is found in the dark spots [21,22]. Comparing the as-bonded and air treated samples, the tiny dark spots grow and spread more for the air treated sample as a result of the thermal treatment. The difference in the interfacial thickness between the air and H_2/H_2O treated samples can be explained by different modes of oxidation. In a Fe–Cr alloy, it has been shown by isotope profiling that external oxidation of chromium occurs in air but internal oxidation of chromium occurs in H_2/H_2O atmosphere [23,24]. A similar process is believed to be present for the Crofer 22 APU/SABS-0 samples. The external oxidation of the Crofer 22 APU alloy elements in air, except for titanium, results in the thicker interface. In the H_2/H_2O atmosphere, internal oxidation [24] along with the lower oxygen partial pressure in the H_2/H_2O atmosphere results in the thinner interface; the granular phases on the Crofer 22 APU alloy side (marked as 4 in Fig. 1(c)) appear due to its interaction with H_2O [25]. The EDS spot analysis shows that the interface mainly consists of Mn–Cr-enriched oxides as supported by the hump near the interface in the chromium concentration profile for the thermally treated samples, the hump at the interface in the manganese concentration profile, and chromium and manganese enrichment at the interface in the EDS maps. For the air treated sample, the diffusivity of iron through the Mn–Cr–enriched interface is higher than that of chromium, resulting in iron-enriched oxides at the interface (marked as 3 in Fig. 1(b)), further supported by the hump in the iron concentration profile on the SABS-0 glass side at the interface, and localized iron-enriched region at the interface in the EDS map [26,27]. In the H_2/H_2O atmosphere, oxygen diffusion towards the interface is dominant than the alloy element diffusion [23,24]. As a result, iron-enriched oxide is absent at the interface.

The interfaces and the bright phases on the SABS-0 glass side for all the samples contain both the Crofer 22 APU alloy and SABS-0 glass elements. This suggests that the chemical reaction between the Crofer 22 APU alloy and the SABS-0 glass occurs during the interface formation, similar to other metal/glass samples [10,11,28–30].

The diffusion distance of iron into the SABS-0 glass increases from the as-bonded, the H_2/H_2O treated, to the air treated samples. The difference between the as-bonded and thermally treated samples is a result of the long thermal treatment time. For the difference between the air and H_2/H_2O treated samples, the higher diffusivity of iron through the interface, as aforementioned, results in the largest diffusion distance for the air treated sample and supported by the presence of iron-enriched oxides at the interface (marked as 3 in Fig. 1(b)), the hump in the iron concentration profile (Fig. 3(a)), and the iron-enrichment in Fig. 5. The chromium diffusion distance increases from the as-bonded, the air treated, to the H_2/H_2O treated conditions in the present study even though it increases from the as-bonded, the H_2/H_2O treated, to the air treated conditions for 100 h thermal treatment time [11]. This anomaly can be explained from the chromium vaporization and the effect of the H_2/H_2O atmosphere. Chromium vaporization occurs in the form of CrO_3 in air and $CrO_2(OH)_2$ in a H_2O-containing atmosphere and increases with oxygen partial pressure and thermal treatment time [31,32]. Low oxygen partial pressure in the H_2/H_2O atmosphere decreases the chromium vaporization rate [33,34]. Accordingly, the chromium diffusion distance is the smallest for the 100 h thermally treated sample. As the thermal treatment time increases, H_2O adsorption at the interface reduces chromium lattice diffusion [35]. At the same time, chromium interaction with water vapor generates fast diffusion paths such as defects and grain boundaries. As a result, chromium diffusion increases, resulting in the larger chromium diffusion distance for the H_2/H_2O atmosphere treated sample in the present study [36–38].

The dendritic phases on the SABS-0 glass side form due to the SABS-0 glass devitrification. Sr^{2+} and La^{3+} ions in the SABS-0 glass are glass modifiers and localized at the atomic level. Also, the SABS-0 glass network structure is perturbed by its chemical reaction with the Crofer 22 APU alloy and the elemental inter-diffusion, in agree-

ment with the EDS spot analysis and localized lanthanum-enriched regions and oxygen accumulation at the interface in the EDS maps. The modifiers and the perturbed network structure promote the devitrification of the SABS-0 glass. Al^{3+} ion is a glass former in the SABS-0 glass, participates in the glass network, and retards the devitrification [16]. Therefore, the devitrified phases have higher strontium and lanthanum contents and lower aluminum content than the darker glass matrix. The different extent of devitrification with different thermal treatment conditions can be understood from the effect of oxygen partial pressure and H_2O interaction with the SABS-0 glass, similar to other silicate glasses [39–41]. Higher oxygen partial pressure accelerates the devitrification of the SABS-0 glass, resulting in the highest extent of devitrification for the air treated sample [40,41]. Incorporation of H_2O in the SABS-0 glass reduces the fraction of non-bridging oxygen, resulting in the lowest extent of devitrification for the H_2/H_2O treated sample [42,43].

4.2. MC Crofer 22 APU/SABS-0 samples

The interfacial behavior of the MC Crofer 22 APU/SABS-0 samples in different atmospheres can be discussed from the combined effect of the Crofer 22 APU alloy oxidation, the stability of the MC layer, the chemical reaction of the MC layer with the Crofer 22 APU alloy and the SABS-0 glass, the diffusion of the related elements, and the SABS-0 glass devitrification.

The formation and growth of the titanium-enriched dark spots are due to the same reasons discussed for the Crofer 22 APU/SABS-0 samples. However, oxygen diffusivity through the $(Mn,Co)_3O_4$ coating is higher than that through the oxide layer for the bare Fe-Cr alloy, which is similar to the Crofer 22 APU alloy [44]. As a result, the internal oxidation is enhanced and the size and spread of the dark spots are larger for the MC Crofer 22 APU/SABS-0 samples.

The interfaces between the Crofer 22 APU alloy and the MC layer (marked as 1 in Fig. 2) are formed by the Crofer 22 APU alloy oxidation as seen from the EDS spot analysis. First, metallic element oxidation contributes to the interface formation. Chromium oxide is the main phase and iron-containing Mn–Cr–O spinel phase may be present [45]. Second, since the bonding of the Crofer 22 APU alloy and SABS-0 glass samples was carried out in argon atmosphere at 960 °C, the MC layer is unstable; Co^{3+} ions in the MC layer are reduced to Co^{2+} ions at low oxygen pressure above 900 °C, resulting in the cobalt-enriched phases, supported by the Mn:Co ratio of ~1:4 in the MC layer [46]. Cobalt diffuses to the interface between the Crofer 22 APU alloy and the MC layer. Subsequently, this interface (marked as 1 in Fig. 2) contains cobalt. Third, manganese diffusion from the Crofer 22 APU alloy to the interface increases with the thermal treatment time and accordingly the amount of the spinel phase increases, supported by the increased Mn:Cr ratio for the thermally treated samples [47]. As a result, the interfacial thickness increases for the thermally treated samples. The thinner interfacial thickness and the appearance of the granular phases for the H_2/H_2O atmosphere treated sample are attributed to the water vapor and the oxygen pressure as discussed for the corresponding bare Crofer 22 APU/SABS-0 sample. Absence of cobalt at the interface for the thermally treated samples is attributed to the decrease of the faster diffusion paths for cobalt due to the spinel phase growth. Iron and chromium diffuse to the MC layer (marked as 2 in Fig. 2(a)) and form solid solution with the spinel phase, resulting in their presence in the MC layer for the as-bonded sample [48]. The interface between the MC layer and the SABS-0 glass (marked as 3 in Fig. 2(a)) forms due to their chemical reaction as seen from the EDS spot analysis. For the air treated sample, the MC layer becomes more unstable, decomposes after the long term thermal treatment [49], and reacts severely with the SABS-0 glass. However, manganese diffuses more than cobalt into the SABS-0 glass as supported by the higher manganese content (Mn:Co = 3:1) at the interface between the MC layer and the SABS-0 glass (marked as 3 in Fig. 2(b)) and the smaller hump width for the cobalt concentration profile. Therefore, the MC layer is thinner and contains higher cobalt along with the SABS-0 glass elements for the air treated sample. For the H_2/H_2O atmosphere treated sample, a new interfacial layer (marked as 5 in Fig. 2(c)) is observed rather than the MC layer and the interface between the MC layer and the SABS-0 glass. The EDS spot analysis shows that this layer is Mn–Cr–O-enriched but the EDS line scan and map analyses show that this layer is also iron-enriched. This means that this layer forms due to the interaction among the Crofer 22 APU alloy, the MC layer, and the SABS-0 glass.

The diffusion distances of iron and chromium into the SABS-0 glass are comparable with the total interfacial thickness for the as-bonded sample but decrease for the thermally treated samples. This means the MC coating on the Crofer 22 APU alloy and its interaction with the alloy and the SABS-0 glass (marked as 2 in Fig. 2(b) and 5 in Fig. 2(c)) hinder the diffusion of iron and chromium into the SABS-0 glass. The hump in the cobalt concentration profile shifts slightly into the SABS-0 glass from the interface, suggesting more cobalt diffusion in the H_2/H_2O atmosphere. Lower oxygen activity in the H_2/H_2O atmosphere increases cobalt diffusion rate [50].

The dendritic phases form on the SABS-0 glass side due to the SABS-0 glass devitrification. The devitrified phases have higher strontium and lanthanum contents but lower aluminum content than the darker glass matrix as explained for the bare Crofer 22 APU/SABS-0 glass. However, the thermal treatment atmospheres do not affect the extent of the SABS-0 glass devitrification. Considering the interfacial morphology, elemental inter-diffusion, and the interfacial phases, it can be concluded that the interfacial stability is higher in the H_2/H_2O atmosphere than in air.

4.3. Influence of interfacial behavior on sealing reliability

Interconnect/seal glass interface plays a crucial role in the sealing reliability. This can be discussed from several aspects: gas leakage, structural integrity, and electrical performance. Cracks and pores at the interface are potential gas leakage sources. These defects form due to the CTE difference among the seal glass, newly formed interfacial species from the reactions, and the metallic interconnect. A SrO–CaO–NiO-Y_2O_3-borosilicate glass reacts with the Crofer 22 APU alloy and forms $SrCrO_4$ of high CTE ($21.0–23.0 \times 10^{-6}\ K^{-1}$). Air atmosphere causes more $SrCrO_4$ formation than H_2/H_2O atmosphere. Subsequently, the gas leakage rate in air is one order of magnitude higher ($3–9 \times 10^{-3}$ sccm cm^{-1}) than that in H_2/H_2O atmosphere ($1–2 \times 10^{-4}$ sccm cm^{-1}) [51]. The interfacial thickness of a BaO–CaO–borosilicate glass with the Crofer 22 APU alloy increases from 10 to 76 μm after 200 h of thermal treatment at 750 °C in air due to the continuous reaction between them. As a result, the rupture strength decreases from ~83 to ~55 kPa [13]. The electrical resistance of an interconnect alloy (similar to the Crofer 22 APU alloy)/BaO–CaO–silicate glass/interconnect alloy tri-layer assembly decreases from 1 kΩ m to <1 Ω m after 400 h of exposure to H_2/H_2O atmosphere from the inside and air from the outside due to the continuous alloy-glass reaction and presence of iron- and chromium-containing conductive oxides at the interface. Electrical failure due to short-circuiting occurs if the conductive interfacial thickness reaches the sealing glass layer thickness [12].

In practice, seal glass layers of a few hundred micron thick are used to join the cell components. In the present study, the interfacial thickness for the Crofer 22 APU/SABS-0 sample increases in air but remains at <2 μm. The diffusion lengths of the Crofer 22 APU elements into the SABS-0 glass are limited to <10 μm. The interfacial thicknesses and the elemental diffusion lengths are almost comparable regardless of the thermal treatment conditions. All these suggest that the interface has promising stability for long term use. The sealing reliability is expected to be similar to or bet-

ter than the AISI 441 alloy/SABS-0 glass/YSZ tri-layer assembly [52] because the interfacial behavior of the AISI 441/SABS-0 sample is inferior to that of the Crofer 22 APU/SABS-0 sample [11]. However, the long term stability of the interface, the interfacial phases, and the electrical resistivity need to be further investigated. The MC Crofer 22 APU/SABS-0 interfaces, on the other hand, contain pores. The MC layer is unstable in the studied conditions and severely reacts with the Crofer 22 APU alloy and the SABS-0 glass. Accordingly, the MC Crofer 22 APU/SABS-0 interface is expected to be problematic for long term sealing although the elemental diffusion lengths are limited to <5 μm.

5. Conclusions

Interfacial compatibility of $SrO–La_2O_3–Al_2O_3–SiO_2$ (SABS-0) seal glass with bare and $(Mn,Co)_3O_4$ coated Crofer 22 APU alloy surfaces has been studied in air and H_2/H_2O atmospheres at 800 °C for 1000 h. The bare Crofer 22 APU/SABS-0 samples show superior interfacial compatibility. The poor stability of the $(Mn,Co)_3O_4$ coating and its severe interaction with the SABS-0 glass degrade the interfacial compatibility of the $(Mn,Co)_3O_4$ coated Crofer 22 APU/SABS-0 samples. For the bare Crofer 22 APU alloy, iron diffusion into the Crofer 22 APU alloy increases in air and chromium diffusion increases in the H_2/H_2O atmosphere. The $(Mn,Co)_3O_4$ coating hinders iron and chromium diffusion into the SABS-0 glass. The interfacial stability is better in the H_2/H_2O atmosphere because of limited alloy oxidation and SABS-0 glass devitrification for the Crofer 22 APU/SABS-0 sample and limited alloy oxidation for the $(Mn,Co)_3O_4$ coated Crofer 22 APU/SABS-0 sample.

Acknowledgements

Financial support from Department of Energy under grant number DE-FC07-06ID14739 is sincerely acknowledged. We thank Dr. Gary Yang, Pacific Northwest National Laboratory, Richland, Washington, USA for providing Crofer 22 APU alloy and Prof. Xingbo Liu, West Virginia University, USA for providing $(Mn,Co)_3O_4$ coated Crofer 22 APU alloy for this work.

References

[1] M.K. Mahapatra, K. Lu, Mater. Sci. Eng. R 67 (2010) 65–85.
[2] Z. Yang, G. Xia, K.D. Meinhardt, K.S. Weil, J.W. Stevenson, J. Mater. Eng. Perform. 13 (2004) 327–334.
[3] Z. Yang, K.D. Meinhardt, J.W. Stevenson, J. Electrochem. Soc. 150 (2003) A1095–A1101.
[4] Z. Yang, J.W. Stevenson, K.D. Meinhardt, Solid State Ionics 160 (2003) 213–225.
[5] K.D. Meinhardt, D.S. Kim, Y.S. Chou, K.S. Weil, J. Power Sources 182 (2008) 188–196.
[6] Y.S. Chou, J.W. Stevenson, P. Singh, J. Electrochem. Soc. 154 (2007) B644–B651.
[7] Z. Yang, Int. Mater. Rev. 53 (2008) 39–54.
[8] Z. Yang, G.G. Xia, X.H. Li, J.W. Stevenson, Int. J. Hydrogen Energy 32 (2007) 3648–3654.
[9] M.K. Mahapatra, K. Lu, Int. J. Appl. Ceram. Technol. 7 (2010) 10–21.
[10] M.K. Mahapatra, K. Lu, J. Mater. Sci. 44 (2009) 5369–5378.
[11] M.K. Mahapatra, K. Lu, J. Am. Ceram. Soc., 2010, in press.
[12] V.A.C. Haanappel, V. Shemet, S.M. Gross, T. Koppitz, N.H. Menzler, M. Zahid, W.J. Quadakkers, J. Power Sources 150 (2005) 86–100.
[13] K.S. Weil, J.E. Deibler, J.S. Hardy, D.S. Kim, G.G. Xia, L.A. Chick, C.A. Coyle, J. Mater. Eng. Perform. 13 (2004) 316–326.
[14] M.K. Mahapatra, K. Lu, Int. J. Hydrogen Energy 35 (2010) 7945–7956.
[15] M.K. Mahapatra, K. Lu, R.J. Bodnar, Appl. Phys. A 95 (2009) 493–500.
[16] K. Lu, M.K. Mahapatra, J. Appl. Phys. 104 (2008) 074910.
[17] J. Wu, Y. Jiang, C. Johnson, X. Liu, J. Power Sources 177 (2008) 376–385.
[18] N.H. Menzler, D. Sebold, M. Zahid, S.M. Gross, T. Koppitz, J. Power Sources 152 (2005) 156–167.
[19] J. Goldstein, D. Newbury, D. Joy, C. Lyman, P. Echlim, E. Lifshin, L. Sawyer, J. Michael, Scanning Electron Microscopy and X-ray Microanalysis, third ed., Springer, New York, 2007, pp. 165–173, 286–295, 391–451.
[20] W.D. Kingery, H.K. Bowen, D.R. Uhlmann, Introduction to Ceramics, second ed., John Wiley and Sons Inc., New York, 1976, pp. 232–264.
[21] P. Kofstad, High Temperature Corrosion, Elsevier Applied Science Publishers Ltd., England, 1988, pp. 324–440.
[22] E.A. Brandes, G.B. Brook, Smithells Metals Reference Book, seventh ed., Butterworth Heinemann, Oxford, 1992, pp. 241–242.
[23] G. Bamba, Y. Wouters, A. Galerie, G. Borchardt, S. Shimada, O. Heintz, S. Chevalier, Scripta Mater. 57 (2007) 671–674.
[24] P. Jussila, H. Ali-Löytty, K. Lahtonen, M. Hirsimäki, M. Valden, Surf. Sci. 603 (2009) 3005–3010.
[25] M.J. Garcia-Vergas, L. Lelait, V. Kolarik, H. Fietzek, M.D. Juez-Lorenzo, Mater. High Temp. 23 (2005) 245–251.
[26] R.E. Lobnig, H.P. Schmidt, K. Hennesen, H.J. Grabke, Oxid. Met. 37 (1992) 81–93.
[27] J. Gilewicz-Wolter, J. Dudala, Z. Żurek, M. Homa, J. Lis, M. Wolter, J. Phase Equilib. Diffus. 26 (2005) 561–564.
[28] J.A. Pask, in: W.E. Moddeman, C.W. Merten, D.P. Kramer (Eds.), Technology of Glass, Ceramic, or Glass–Ceramic to Metal Sealing, The American Society of Mechanical Engineers, New York, 1987, pp. 1–7.
[29] P. Kumar, V.A. Greenhut, Metal–Ceramic Joining, TMS Minerals, Metals, Materials, Warrendaley, PA, 1990, pp. 3–11.
[30] A.J. Sturgeon, D. Holland, G. Patridge, C.A. Elyard, Glass Technol. 27 (1986) 102–107.
[31] Y.W. Kim, G.R. Belton, Metall. Mater. Trans. B 5 (1974) 1811–1816.
[32] C. Gindorf, L. Singheiser, K. Hilpert, J. Phys. Chem. Solids 66 (2005) 384–387.
[33] B.B. Ebbinghaus, Combust. Flame 93 (1993) 119–137.
[34] M. Stanislowski, E. Wessel, K. Hipert, T. Markus, L. Singheiser, J. Electrochem. Soc. 154 (2007) A295–A306.
[35] S.R.J. Saunders, M. Monteiro, F. Rizzo, Prog. Mater. Sci. 53 (2008) 775–837.
[36] E. Park, B. Huning, H.J. Grabke, M. Spiegel, Defect Diffus. Forum 237–240 (2005) 928–933.
[37] P. Kofstad, Oxid. Met. 44 (1995) 3–27.
[38] D.J. Young, Mater. Sci. Forum 595–598 (2008) 1189–1197.
[39] T. Jin, K. Lu, J. Power Sources 195 (2010) 195–203.
[40] R. Müller, E.D. Zanotto, V.M. Fokin, J. Non-Cryst. Solids 274 (2000) 208–231.
[41] G. Patridge, P.W. McMillan, Glass Technol. 15 (1974) 127–133.
[42] D.R. Wolters, H. Verweij, Phys. Chem. Glass. 22 (1981) 55–61.
[43] H. Chen, J.W. Park, Phys. Chem. Glass. 22 (1981) 39–42.
[44] T. Horita, H. Kishimoto, K. Yamaji, Y. Xiong, M.E. Brito, H. Yokokawa, Y. Baba, K. Ogasawara, H. Kameda, Y. Matsuzaki, S. Yamashita, N. Yasuda, T. Uehara, Solid State Ionics 179 (2008) 2216–2221.
[45] C.L. Chu, J.Y. Wang, R.Y. Lee, T.H. Lee, S. Lee, J. Fuel Cell Sci. Technol. 6 (2009) 031013.
[46] S. Naka, M. Inagaki, T. Tanaka, J. Mater. Sci. 7 (1972) 441–444.
[47] Z. Yang, J.S. Hardy, M.S. Walker, G.G. Xia, S.P. Simmer, J.W. Stevenson, J. Electrochem. Soc. 151 (2004) A1825–A1831.
[48] J. Wu, C.D. Johnson, R.S. Gemmen, X.B. Liu, J. Power Sources 189 (2009) 1106–1113.
[49] C.C. Mardare, M. Spiegel, A. Savan, A. Ludwig, J. Electrochem. Soc. 156 (2009) B1431–B1439.
[50] F.H. Lu, R. Dieckmann, Solid State Ionics 67 (1993) 145–155.
[51] Y.S. Chou, J.W. Stevenson, R.N. Gow, J. Power Sources 170 (2007) 395–400.
[52] M.K. Mahapatra, K. Lu, Fuel Cells, in press.